Performance Investigation of PV Battery Integrated Parallel Operated Inverters in Standalone Mode

Sravanthy Gaddameedhi iD *, E. Vidya Sagar iD **, N. Susheela iD **

*Department of Electrical Engineering, Sreenidhi Institute of Science and Technology, Hyderabad, Telangana, 501301.

**Department of Electrical Engineering, Osmania University, Hyderabad, Telangana.

(sravanthi314@gmail.com, vidyasagar.e@uceou.edu, nsusheela2007@yahoo.com)

‡
Corresponding Author: Sravanthy Gaddamedhi, Sreenidhi Institute of Science and Technology, Tel: 8919787765, sravanthi314@gmail.com.

Abstract: The Integration of non-conventional energy systems (NCES) like solar, wind, etc., into the grid with power electronic devices is adapted to meet the demand. Parallel connection of inverters (PCI) is an efficient method to boost power handling capacity, reliability, and system efficiency. However, the main drawback is the unequal power sharing among the inverters while using the conventional droop control technique (CDC). In addition, the circulating currents (CC) flow between these PCI, leading to common mode voltage (CMV), current waveform distortion, and reduction in the system's overall performance. This work consists of a photovoltaic system (PV) and battery energy storage system (BES) as the Distributed generation (DG) unit to voltage source inverter (VSI) 1 and 2. The multi-objectives of the suggested work are (a) the equal power/load sharing among two inverters, (b) effective minimization of CC and the CMV, (c) maintaining constant DC-Link (DCL) voltage during different solar irradiation and constant temperature, and (d) the reduction in total harmonic distortion (THD) of load current. A novel approach related to the enhanced droop control (EDC) method with an artificial neural network controller (ANNC) was suggested here to overcome the above issues. The performance analysis of the suggested technique was done in the Matlab/ Simulink platform with two test studies for different loads. A comparative analysis with the available methods like the Proportional integral Controller (PIC) and Sliding Mode Controller (SMC) was carried out to exhibit the viability of the developed control technique. The THD is effectively diminished to 1.18% and 2.3% for the two test case studies of the proposed method, which are much lower than those of existing methods available in the literature.

Keywords- Parallel inverter, Power sharing, circulating current, Common mode voltage, PVS, BES

1. Introduction

Recently, the association of NCES is appearing in the form of microgrids to have a reliable power supply. However, they are connected to the distribution network via inverters, particularly when operating in parallel as islanded systems. In the islanding operation of the micro-grid, the DGs are typically linked to an AC distributed system through inverters. To address these challenges, various techniques have been developed for controlling the parallel operation of inverters and specifically for uniform power sharing by combining different control schemes.

1.1 Motivation and Background

The PCI associated with renewable sources is encouraged due to its advantages like increased power handling capacity, reduced conversion stress, and increased efficiency, reliability and wide applications towards various speed controls of motor drives. However, an essential issue with PCI is the unequal distribution of power among the inverter's due variation in the parameters, communication delays, controller design differences, inverter capacity disparities, non-identical loads and line impedance etc. Additionally, it generates flow of CC which occurs due to the mismatching in impedances among the inverter, switching frequency, dead time, etc., which leads to the generation of current waveform imperfections, CMV and a decrease in the overall efficiency of the system.

1.2 Literature Survey

A nonlinear sliding mode controller was described for parallel-operated multilevel inverters to minimize circulating currents, current distortion, and unbalanced load sharing. In addition, experimental investigation results were exhibited to show the superiority of the suggested method [1]. An FFNN for accurate power sharing in parallel connected inverters controls the voltage and frequency in an islanded microgrid, including PVS, BES, and SOFC, compared to the CDC [2]. The hybrid PI and nonlinear SMC controller are suggested to effectively minimize the CC in PCI [3]. The virtual impedance and compensating voltage have been considered for maintaining the micro-grid voltage and frequency with different impedances and droop gains in the single and multi-

bus models. THD is also reduced for various nonlinear unbalanced loads within the IEEE standard values [4]. Different concepts and controlling methods of PCI for uniform load sharing among the individual inverter and retaining voltage and frequency values within permissible limits. Comparison analysis was also done for each technique in terms of their advantages and disadvantages [5].

The Space Vector Pulse Width Modulation technique (SVPWM) was adapted to minimize the CC and CMV in PCI for smooth and effective operation. Mainly, in this technique, large, medium, small and zero vector modulation has been considered, and the suggested method's results are compared and analyzed with conventional PWM methods [6]. Furthermore, a fuzzy logic controller is designed and analyzed in PCI to improve its performance and efficiency by reducing the circulating currents flowing through the Parallel connected paths. As a result, this suggested configuration's performance is more efficient than the conventional PI controller [7]. Different types of linear and nonlinear droop control techniques are discussed to improve the performance of load equal sharing, stability analysis, THD, steady-state, and transient analysis of inverters connected in Parallel in the distribution system. It also focuses on the power quality (PQ) issues with obtaining the required output with low THD using different control strategies [8]. This paper recommends an adaptive droop control algorithm for eliminating CC in a low-voltage DC micro-grid. It also suggests the second controller is used to determine line resistances through mathematical calculations, and consequently, the droop parameters are also adjusted [9]. This paper mainly focuses on the capability of power sharing among parallel distributed generators (DGs). It also describes the analysis and control of PCI. Here a novel EDC is introduced for frequency restoration and voltage control among the distributed generators over droop control characteristics [10].

A novel algorithm derived from soccer league dynamics has been employed to fine-tune an optimal hybrid controller for a UPQC linked with solar power and battery storage systems to enhance the power quality, reduce THD and maintain voltage across DCL capacitor [11]. A self-tuning filter featuring a unit vector generation scheme (STF-UVGS) has been developed. This filter serves the dual purpose of preserving phase synchronization in the series and shunt filters, while also ensuring exceptional system performance across diverse uncertain scenarios, including supply voltage imbalances and distortions [12]. The improved droop control technique provides accurate power sharing in PCI, even if the time delay does not affect the load variation. An experimental setup was also provided to validate the simulation results [13]. A dual control strategy consisting of PQ control and droop control techniques is suggested for the Ac micro-grid to control the output real and reactive powers along with grid voltage and frequency [14]. Virtual impedance based PLL is presented to analyze the PCI efficiently and compensate for the improper power sharing. The proposed scheme improves synchronization and decoupling between the active/reactive power and transient response. It also eliminates power calculations, unlike the CDC technique [15]. Effective suppression of CC in multi-parallel inverters under unbalanced operating conditions is recommended with a

coordinate control strategy based on SVPWM and zero vector feed-forward method [16]. The hybrid technique, which contains the control strategies of virtual impedance (VI) and CDC techniques, is presented to minimize cross and zero-sequence circulating currents in multi-parallel inverters with linear and nonlinear loads [17].

A new dead-beat controller method was developed for the CC minimization in 3Ø PCI to regulate the overlapping time of vectors in each SVPWM. However, the comparison was carried out with the conventional PI control method [18]. The practical control strategy is presented to reduce the improper reactive power sharing among the PCI due to mismatched output impedances. A low pass filter (LF) is also designed to minimize the bandwidth and stabilize the system [19]. A modified droop control technique was investigated with solar powered micro-grid. In this work, the proposed controller achieves equal real and reactive power sharing between solar-powered inverters at different load conditions [20]. The hybrid control method facilitates smooth shifts between the grid integrated mode and islanding mode, and vice versa. This ensures a seamless transition between these modes without the need to reorganize the control structure [21]. To calculate optimal droop parameters and to decrease line impedance for uniform power sharing, a Particle swarm-optimization-based technique was adopted [22].

A direct power control (DPC) strategy is developed to infuse generated solar energy into the electrical network. This injection aligns with a reference design aimed at eliminating reactive power and harmonics originating from nonlinear loads. [23]. This article provides explanations of these renewable energy sources, Maximum Power Point Tracking (MPPT) techniques, and hybrid systems. [24]. Model for a microgrid featuring a solar power system with maximum power point tracking (MPPT) and a battery energy system is presented. A Boost converter is utilized to match the voltage level with the MPPT [25]. Boosting the power capacity of the current grid system and integrating renewable energy sources are essential. Consequently, this study tackles the necessity of employing intelligent techniques to effectively link renewable energy sources to the grid. [26]. This article introduces an elaborate computational model for organic photovoltaic (OPV) cells, specifically based on a single-diode framework. These cells utilize organic semiconductor materials, offering advantages in terms of cost and weight compared to traditional PV cells. [27].

The analysis of the literature above indicates that each approach possesses distinct limitations. These include mostly conventional techniques/controllers are used to address the PCI-related problems, focused on single objective, etc. Hence in this approach solar battery integrated PCI with an enhanced droop control technique and ANNC controller was adopted to investigate its performance.

1.3 Research Gap

However, based on the literature survey, it is evident that the majority of research papers primarily focused on single objectives, such as equal power sharing, reduction of CC's, CMV, and THD reduction, as well as DCL voltage regulation,

with the use of various controllers. In contrast, the proposed work takes a more comprehensive approach by considering not only power sharing but also addressing the reduction of CC's and CMV, along with DCL voltage balancing for different types of loads under varying solar irradiation conditions.

1.4 Contributions

The key highlights of this article are as follows:

- The main objectives of the proposed method are to achieve uniform power sharing, minimize CC, CMV, and maintain constant DCL voltage.
- Development of an ANN controller for Solar PV and BES integrated with PCI (PCI-SBS).
- Results are obtained for various loads under varying solar irradiation and constant temperature conditions.
- The performance analysis was conducted with standard controllers like PIC and SMC, and a comparison was made to demonstrate the superiority of the proposed technique over existing methods in the literature.

1.5 Organization of the Paper

The proposed paper focuses on the analysis of ANNC for a solar battery integrated PCI-SBS. Section 2 provides details about the configuration, and operation of PCI-SBS, including the controllers for solar and battery. In Section 3, conventional and enhanced droop control methods are discussed, while Section 4 introduces the artificial neural network controller. Finally, Section 5 presents the simulation results.

2. Configuration of Proposed PCI-SBS

The structure of the proposed PCI-SBS comprises two VSI's connected in Parallel shares the common load integrated with micro-grid, a combination of PVS and BES, shown in Fig.1. The dc side of VSI1 and VSI2 are connected to the PVS via micro-grid, a combination of PVS and BES, shown in Fig.1.
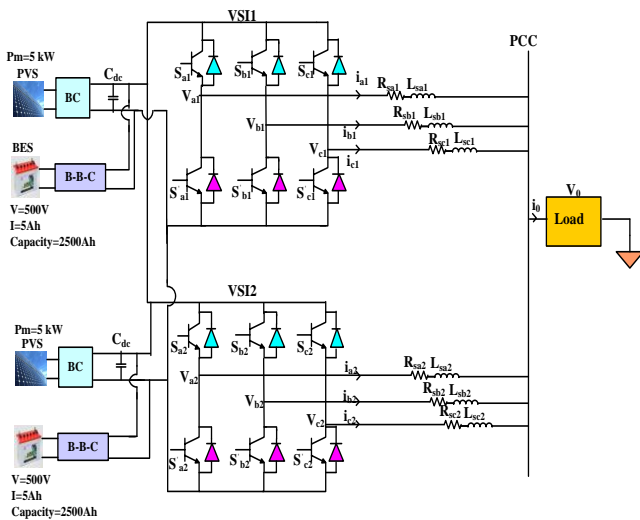
Fig.1. Block diagram of the proposed configuration

The dc side of VSI1 and VSI2 are connected to the PVS via DC-DC boost converter (BC) and BES connected through DC-DC buck boost converter (B-B-C) to assist the battery's necessary charging and discharging modes. In addition, the battery aims to maintain constant DCL voltage. Therefore, various loads are chosen to investigate the performance of the proposed configuration.

The PVS and BES externally support the DCL of PCI through a B-C and B-B-C to regulate the voltage across DCL is constant during various loads of different solar irradiation and to reduce the ratings of converters. The PVS and BES ratings considered in this work are given in Table-1. The dispersion of power for the proposed PCI-SBS at the DCL is exhibited by Eq. (1), and the corresponding flow chart is shown in Fig. 8.

$$P_{PVS} + P_{BES} - P_{DCL} = 0 \quad (1)$$

2.1 Solar Modelling

The PV cells are connected in series to form a string and some of such strings are in parallel to produce the necessary amount of voltage and current. In the module, every PV cell is modeled by a diode in parallel with the current source as shown in Fig 2. The model of the PV system with a boost converter is shown in Fig.3.

It consists of a photo current source (i_{ph}) with a forward diode carrying current (i_d), a series, and parallel cell resistances ($R_{s,PV}$ and $R_{sh,\ PV}$) carrying a current of (i_{PV}, $i_{sh,PV}$). The PV cell identifies sun irradiation and converts it into current. By adopting KCL, PV cell output current (i_{PV}) is obtained by Eq. (2)
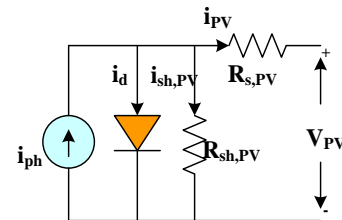

Fig.2. PV cell model

$$i_{PV} = i_{ph} - i_d - i_{sh} \quad (2)$$

By, substituting expressions for i_d, i_{sh}, the PV module output current is obtained is given by Eq. (3)

$$i_{PV,m} = i_{ph} - i_{S,PV}\left[\exp\left(\frac{Q(V_{PV} + (i_{PV,m}R_{S,PV}))}{\eta k T_C}\right) - 1\right] - \frac{V_{PV,m} + (i_{PV,m}R_{S,PV})}{(R_{sh,PV})} \quad (3)$$

Where, $i_{PV,m}$, $V_{PV,m}$ is the module current and voltage, $i_{s,PV}$ is the reverse saturation current, Q is the electron charge, η is the diode ideal factor, k Boltzmann's constant, and T_C denotes the cell temperature, and N_s is series connected PV cell. The PV modules are connected in series and parallel to form an array by Eq. (4)

$$i_{PV,m} = i_{ph}N_p - i_{S,PV}N_p\left[\exp\left(\frac{Q(V_{PV} + N_s/N_p(i_{PV,m}R_{S,PV}))}{N_s\eta k T_C}\right) - 1\right] - \frac{V_{PV,m} + N_s/N_p(i_{PV,m}R_{S,PV})}{N_s/N_p(R_{sh,PV})} \quad (4)$$

Where,

$$i_{ph} = (i_{ph,n} + K_1 \Delta T_C) \frac{G}{G_n} \quad (5)$$

Where, G, G_n represents solar irradiance (W/m²) and at STC, ΔT_C variation in temperature. The maximum output power of PV ($P_{PV\max}$) is calculated by Eq. (6). The PV cell characteristics for various irradiations and temperatures are exhibited in Fig. (4) and (5) respectively.

$$P_{PV\max} = V_{PV\max} \times i_{PV\max} \quad (6)$$

2.2 Battery Energy Storage System (BES)

The battery system is connected to the DCL of PCI via B-B-C and its controller is given in Fig.6. The Battery consists of several cells which are arranged in series/parallel in order to obtain necessary voltage and current. In this work, the Li-ion battery is selected from the Simulink library due to its advantages like slow discharge and low maintenance cost. The charging or discharging form of the Li-ion battery is represented in Eq. (7)

$$V_b = E_{f1,2}(i_t, i_h, i_b) - iR \quad (7)$$

Where, $E_{f1,2}$ (i_t, i_h, i_b) is no-load voltage, R is the internal resistance, i_b battery current. The battery constant voltage E_0 and battery capacity Q is expressed by Eq. (8).
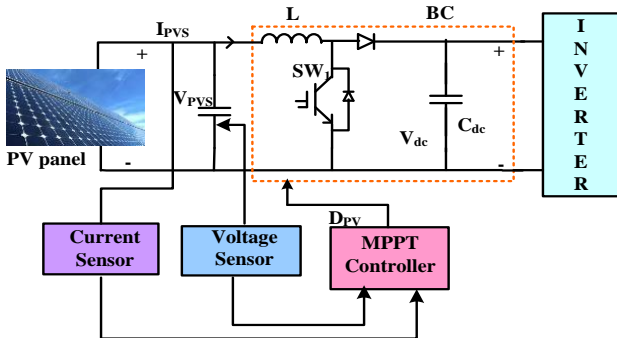
Fig.3. Modeling of PV system

$$E_{f1}(i_t, i_h, i_b) = E_0 - K(\frac{Q}{0.1Q + i_t})i_h - K(\frac{Q}{Q - \int i_t dt})i_t + A\exp(-B.\int i_t dt) \quad (8)$$

$$E_{f2}(i_t, i_h, i_b) = E_0 - K(\frac{Q}{Q + i_t})i_h - K(\frac{Q}{Q - \int i_t dt})i_t + A\exp(-B.\int i_t dt)$$
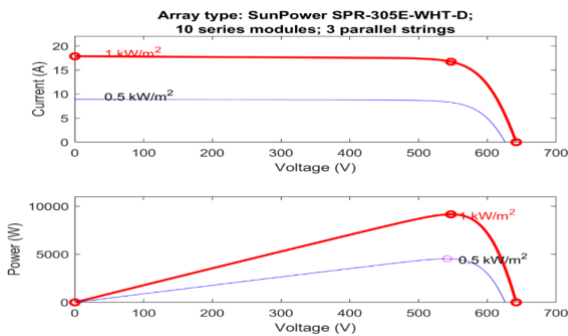
Fig. 4. PV cell characteristics at various irradiation and constant temperature 25⁰c
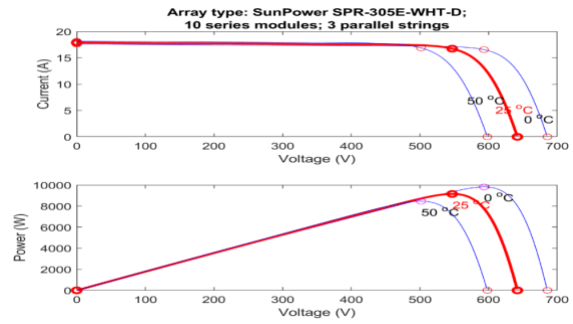
Fig.5. PV cell characteristics at various temperature and constant irradiation

The state of charge of the battery (*SOCOB*) is expressed in Eq (9).

$$SOCOB = 80(1 + \int i_{BES} dt Q) \quad (9)$$

The PV will decide whether, the battery to charge or discharge while satisfying the constraints given by Eq. (10). The battery discharge characteristics are shown in Fig. 7.
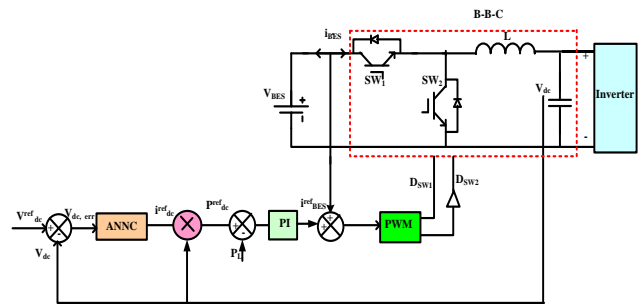
$$SOCOB_{\min} \leq SOCOB \leq SOCOB_{\max} \quad (10)$$

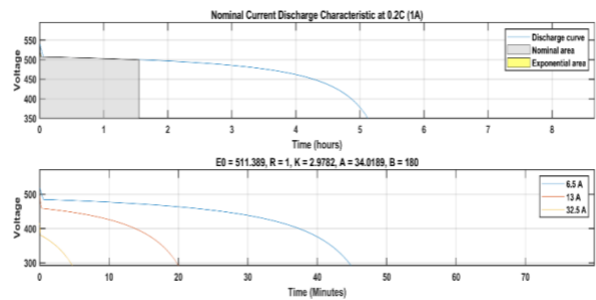**Fig.6**. Modeling of the Battery system

Fig. 7. Li-ion battery characteristics

Table 1: PV and BES specifications

Device	Parameters	Values
PV panel (Sun Power SPR-215-	Output Power	305.226W
	Open-circuit-voltage	64.2V
	Short circuit current	5.96A
	Under max power, the V & I	54.7V /5.58A
	Number of PV cells assembled in series and parallel	10 and 3

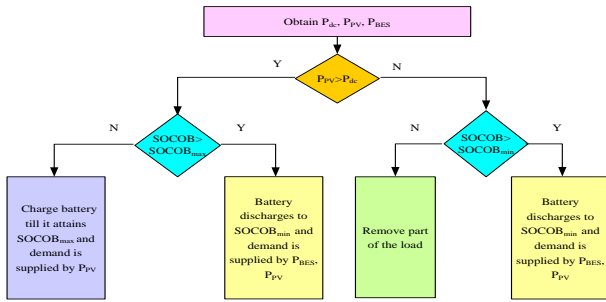| WHT-U)	R_{PVS}, L_{PVS} and C_{PVS}	0.005Ω, 5mH and 10µF
Battery	Rated capacity	5Ah
	Maximum capacity	2250 Ah
	Nominal voltage	500 V
	Fully charge voltage	544.4V
	L_{BES} and C_{BES}	0.35mH and 250µF

Fig.8. Power balance system

3. Control Strategy

3.1 Conventional Droop Control Technique (CDC)

To control the active and reactive powers of a distribution system, the CDC technique is employed [2]. Generally, the active and reactive powers are controlled through angular frequency and voltage given by Eq. (11 &12).

$$\omega = \omega^* - m(P_{cal} - P^*) \quad (11)$$

$$E = E^* - n(Q_{cal} - Q^*) \quad (12)$$

P^* and Q^* are the rated real and reactive powers; m and n are the inverter droop coefficients for frequency and voltage, respectively; ω^* is the nominal angular frequency; and E^* is the nominal voltage. The block diagram of CDC is shown in Fig. 9.

3.2 Enhanced Droop Control Technique (EDC)

This research paper introduces an Enhanced Droop Control (EDC) technique as an alternative to address the limitations of the Conventional Droop Control (CDC) technique. Fig.10 illustrates the functional diagram of EDC, revealing the relationship between the active power and frequency control and the relation between the reactive power and voltage control. In order to enhance frequency accuracy, a frequency restoration scheme (FRS) is employed, wherein the frequency value is reset to its nominal rated value ω∗. The analysis of this method incorporates the inclusion of Δω term in Eq. (11).

$$\omega_{new} = \omega^* + \Delta\omega - m(P_{cal} - P^*) \quad (13)$$

For steady-state operation $\Delta\omega$ is reformed as:

$$\frac{d}{dt}(\Delta\omega) = K\Delta\omega \quad (14)$$

Where $\Delta\omega$ is the error in the frequency. The constant K monitors frequency of the system.

However, the FRS is analyzed by taking the Laplace transform of Eq. (13) and (14) and the new reactive power of the inverter obtained from EDC is given by Eq. (15)

$$E_{new} = \Delta E - n(Q_{cal} - Q^*) \quad (15)$$

Where ΔE is the drop in voltage which is provided by

$$\Delta E = E^* - E \quad (16)$$

By considering constant K, the ΔE can be rewritten as

$$\Delta E = K(E^* - E) \quad (17)$$

The control of VSI involves three loop controls which are an outer loop for power control, a middle loop for control of voltage and an inner loop for current control. However, by using the inverter output voltage and current signals, the active and reactive powers are calculated [2].
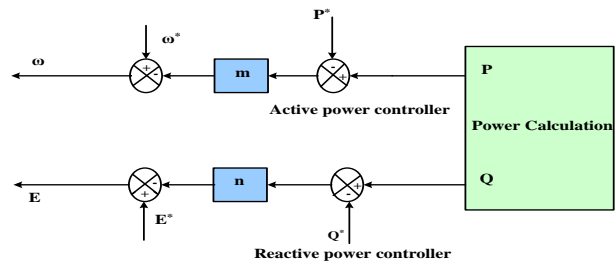

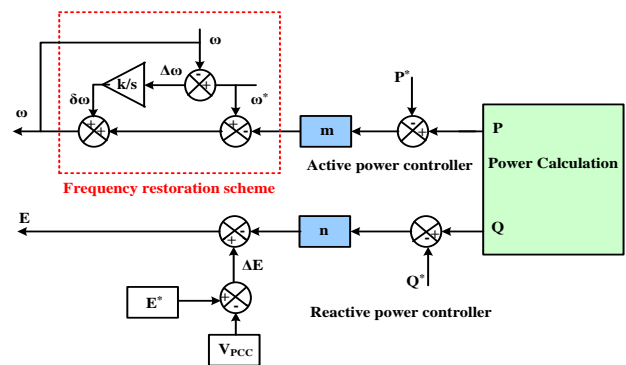**Fig.9.** Droop controller block diagram

Fig.10. Enhanced Droop Control Method

The resultant output voltage from SRF is given to the inverter. Then, this is fed to the droop controller to get the variables such as E new and ω new. Later the SRF $V_{ref} = \sin\theta$ is developed using E new and ω new. Finally, this reference voltage is given to the PWM generator to produce proper pulses for the inverter. The ratings of proposed configuration are exhibited in table.2.

Table 2: Ratings of the developed system

Parameter	Value
DC supply	700 V
Rated AC voltage	380 V
Carrier frequency	10 kHz
P_F, Q_E Co-efficient	m= 1e-5, and n = 2e-4

Filter Inductance	3mH
Filter Capacitance	10μF
Resistance of LC Filter	0.2Ω
Inner current loop	K_p=0.01, & K_i=50
Outer voltage loop	K_p=0.05, & K_i=100
Nominal Frequency	50Hz
DCL capacitance	350μF

3.3 ANN Controller

ANN is the trending intelligence controller whose work is inspired by the behavior of the human brain with the advantage of self-adapting unique techniques. Multilayer perceptions (MLP) are famous in ANNC. Therefore, it is very suitable for power controllers. The structure of ANNC contains an input layer (IL), a hidden layer (HL) and an output layer (OL) shown in Fig.11. The input data is stored in IL and moves to HL. Later, it multiplies with weights on the links, which are present between IL and HL. Usually, calculations are done in HL, whereas OL gives the results.

The given input signal passes through network layer by layer. The links between each neuron are weighted. Here, W_{ih} represents the weight between input and hidden layer, W_{ho} represents weights between hidden and output layer. These weights are adjusted during the training process. The hidden layer neurons use non-linear tangent-sigmoid activation function and the output layer neuron uses pure linear activation function. These ae mathematically expressed by the following equations:

$$\phi_h = \frac{2}{1+e^{(-2(w_{ih}*x_i+b_{ih}))}} - 1, i = 1,2 \, and \, h = 1,2,...10 \quad (18)$$

$$Y_1 = W_{ho}*\phi_h + b_o, h = 1,2....10 \quad (19)$$
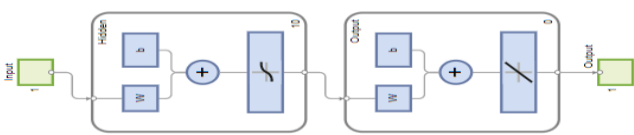
Fig. 11. Structure of ANNC

In this work, Feed-forward artificial neural network is adapted to obtain the constant DCL voltage across microgrid and whose structure is given in Fig.12. During the training the link of weights is updated automatically. The training process is carried out to minimize errors and obtain the desired output.

By analyzing the regression plot displayed in Fig.13 and taking into account the co-relation co-efficient value R, it becomes evident that the FFNN has been successfully trained using the provided training datasets. The testing, validation, and overall system performance are also deemed satisfactory. An R value of 1 indicates perfect correlation. Based on this training process, the performance of the suggested controller is verified in an islanded microgrid system that is being considered.
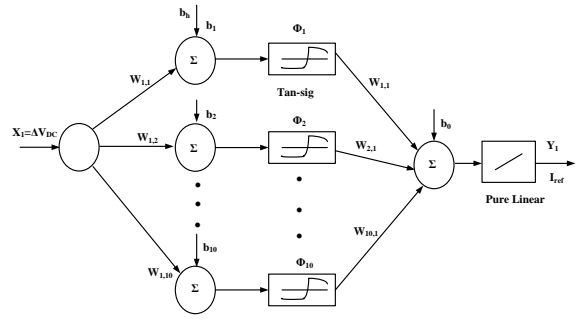

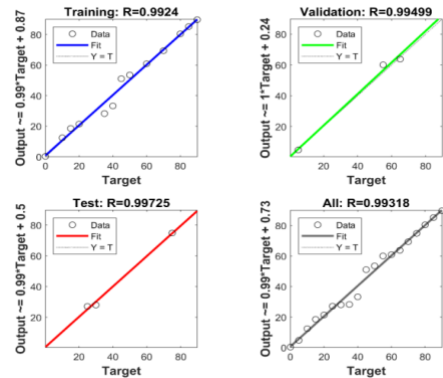**Fig. 12.** Feed-forward artificial neural network for DCL

Fig. 13. Regression plot of ANN controller

3.4 Circulating Currents (CC) and Common Mode Voltage (CMV)

The equivalent circuit of the proposed PCI connected to the common load with impedances Z_1 and Z_2 is as shown in Fig. 14. The currents flowing through the two inverters are I_1 and I_2 respectively given as:

$$I_1 = \frac{E_1 - V_0}{Z_1} = \frac{U_{\Delta 1}}{Z_1} \quad (20)$$

$$I_2 = \frac{E_2 - V_0}{Z_2} = \frac{U_{\Delta 2}}{Z_2} \quad (21)$$

Where E_1, E_2, V_0, Z_1 and Z_2 are the output voltages of inverter1 and 2, load voltage, and system impedance of inverters 1 and 2, respectively.
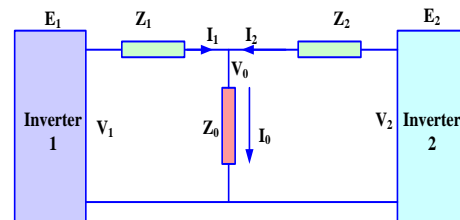

Fig.14. Two Parallel Connected inverters

The load voltage can be derived using Millman'stheorem:

$$V_0 = \frac{\frac{E_1}{Z_1}+\frac{E_2}{Z_2}}{\frac{1}{Z_1}+\frac{1}{Z_2}+\frac{1}{Z_0}} = \frac{Z_0(E_1Z_2+E_2Z_1)}{Z_1Z_2+Z_2Z_0+Z_1Z_0} \quad (22)$$

Where Z_0 is the impedance of the load. Here, CC is represented by

$$I_{cc1} = \frac{I_1 - I_2}{2} \quad (23)$$

In another way, the CC is also defined as

$$I_{cc2} = \frac{I_2 - I_1}{2} \quad (24)$$

Substituting (20), (21) in (23) and (24) results in

$$I_{cc1} = \frac{U_{\Delta 1}Z_2 - U_{\Delta 2}Z_1}{2Z_1 Z_2} \quad (25)$$

$$I_{cc2} = \frac{U_{\Delta 2}Z_1 - U_{\Delta 1}Z_2}{2Z_1 Z_2} \quad (26)$$

The CC of each inverter can be obtained by the difference between the output current and average current given in Eq. (27) -(28).

$$I_1 - I_{Avg} = \frac{2I_1 - I_2 - I_1}{2} = \frac{I_1 - I_2}{2} = I_{cc1} \quad (27)$$

$$I_2 - I_{Avg} = \frac{2I_2 - I_1 - I_2}{2} = \frac{I_2 - I_1}{2} = I_{cc2} \quad (28)$$

The CC can effectively have reduced by using modified SVPWM technique [1]. This modification involves the introduction of a control variable, denoted as K, to regulate the distribution of time duration associated with zero vectors.

CMV is the average instantaneous voltage in a 3Ø inverter. From Fig.15, the CMV is described as the voltage at the DC's center point as O1. If impedance path exists from AC side to O1 via ground, CM voltage will be able to generate CM current.
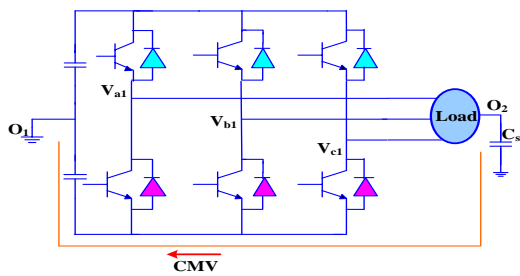
Fig.15. 3Ø VSI with its CMV

$$V_{cn} = 1/3(V_{a01} + V_{b01} + V_{c01}) \quad (29)$$

4 Results and Discussions

The proposed PCI-SBS was developed in MATLAB Simulink environment given in Fig.16 and the sub system diagram for solar and battery is exhibited in Fig. 17 respectively. The inverter1 and inverter2 output voltage/current, voltage and current at the load terminals, active/reactive power sharing, the circulating current and common mode voltages were analyzed. In addition, the THD was also obtained for the proposed system and further, it is compared with those of PIC and SMC, as illustrated in Table.4.
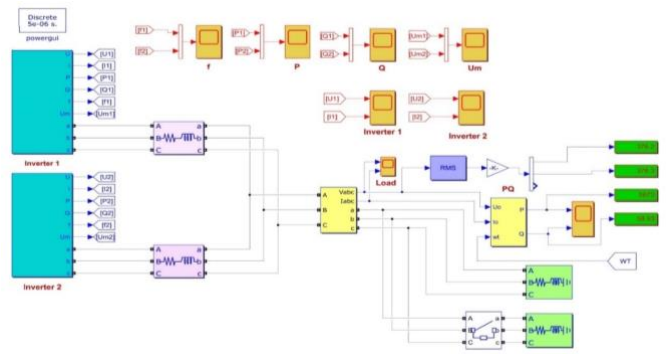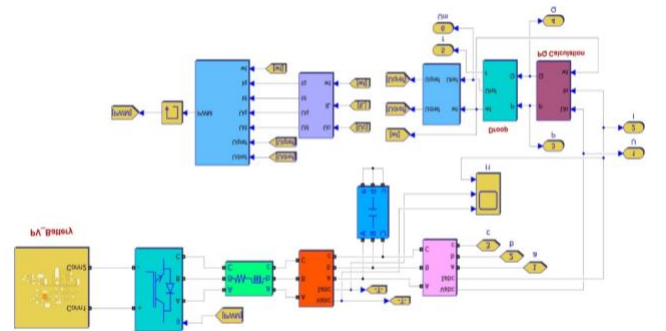

Fig.16. PCI-SBS model in Simulink

Fig.17. Simulink diagram for PVS and BES system

Case 1: Solar irradiation of 1000W/m² and at constant Temperature of 25⁰C:

In the given scenario's, two loads are considered along with two inverters and a solar battery system.

Scenario 1: Performance analysis of proposed method with total 8 kW load:

Load 1: Active Power (P) = 5 kW, Reactive Power (Q) = 500 VAR, active from 0 to 0.5 seconds.

Load 2: Active Power (P) = 3kW, Reactive Power (Q) = 300 VAR, active from 0.5 seconds

The output voltage and current waveforms for inverter 1 and inverter 2 are shown in Fig. 18(a) and Fig. 18(b), respectively. The load voltage and current waveforms are shown in Fig. 18(c). Fig. 18(d) provides the total active and reactive powers at the load Fig. 18(e) and Fig. 18(f) demonstrate that the proposed control method ensures equal sharing of real and reactive powers among the inverters, even during the load change at time t = 0.5 seconds. The Fig. 18 (g) provides the frequency waveform of inverter 1 and 2. Additionally, Fig. 18(h) indicates that the suggested method maintains a constant DCL voltage with a variation in the load. It is also observed that the battery is in charging mode since the solar power exceeds the load power.

Scenario 2: Performance analysis of proposed method with total 15 kW load:

Load 1: Active Power (P) = 5 kW, Reactive Power (Q) = 500 VAR, active from 0 to 0.5 seconds.

Load 2: Active Power (P) = 10 kW, Reactive Power (Q) = 1000 VAR, active from 0.5 seconds

The voltage and current at the load are shown in Fig. 19(a). By examining Fig. 19(a), we can note that the load current escalates from 20A to 30A with the progressive increment of the load. The total active and reactive powers are displayed in Fig. 19(b). From Fig. 19(c) and Fig. 19(d), it can be observed that the proposed control method ensures equal power sharing between the two inverters, even during the load change at time t = 0.5 seconds. Furthermore, the proposed method exhibits its superior performance in regulating DCL voltage as constant. In this case, the battery starts discharging power at t = 0.5 seconds since the load power exceeds the solar power, as depicted in Fig. 19(e). The settling time for the system is low, indicating a fast response to changes.

Case 2: Solar irradiation 800W/m² and at constant Temperature of 25⁰C:

Here also, two loads are considered along with two inverters and a solar battery system.

Scenario 1: Performance analysis of proposed method with total 7 kW load:

Load 1: The active power (P) is 5 kW, and the reactive power (Q) is 500 VAR, and it remains active from time 0 to 0.5 seconds.

Load 2: The active power (P) is 2 kW and the reactive power (Q) is 200 VAR, and it becomes active from 0.5 seconds onward.

The load voltage and current waveforms are shown in Fig. 20(a). Fig. 20(b) provides the total active and reactive powers are available at the load. Fig. 20(c) and 20(d) demonstrate that the proposed control method ensures an equal distribution of real and reactive powers among the inverters, even during the load change that occurs at time t = 0.5 seconds. Furthermore, Fig. 20(e) shows that the suggested method maintains a constant DCL voltage even when there are variations in the load despite a decrease in solar irradiation from 1000 W/m² to 800 W/m², the battery remains in the charging mode as the solar power exceeds the load power.

Scenario 2: Performance analysis of proposed method with total 13 kW load:

Load 1: The active power (P) is 5 kW, and the reactive power (Q) is 500 VAR, and it remains active from time 0 to 0.5 seconds.

Load 2: The active power (P) is 8 kW, and the reactive power (Q) is 800 VAR, and it becomes active from 0.5 seconds onward.

Fig. 21(a) illustrates the voltage and current at the load, revealing a noticeable increase in load current from approximately 12A to 24A. The total active and reactive powers are depicted in Fig. 21(b). By examining Fig. 21(c) and 21(d), we can observe that the proposed control method provides an equal sharing of power between the two inverters, even during the load change that occurs at time t = 0.5 seconds. Furthermore, the proposed method works efficiently in maintaining a stable DCL voltage even during load changes. In this case, the battery starts discharging power at t = 0.5 seconds since the load power exceeds the solar power, as depicted in Fig. 21(e). The suggested method able to

quickly settle the DCL voltage to the steady-state around 0.05 sec and maintain the voltage as constant.

Overall, the proposed controller with the solar battery system effectively handles load changes and ensures equal power sharing among the inverters. The battery operation varies between charging and discharging depending on the power balance between the solar system and the load.

Moreover, through the utilization of the SVPWM technique [1], the suggested PCI-SBS provides a commendable reduction in circulating currents and common mode voltage waveforms, as depicted in Fig. 22 and Fig. 23. The circulating currents were effectively diminished from 10A to 3A, while the common mode voltage exhibited a decrease from 700V to 350V. Additionally, Fig. 24 presents the THD spectrum for the two conducted test studies. By utilizing the proposed technique leads to significant decreases in THD: a reduction from 4.21% to 1.18% in case 1 and from 4.79% to 2.30% in case 2, when compared against the conventional PI-C and SMC methods and it is given in table.3.
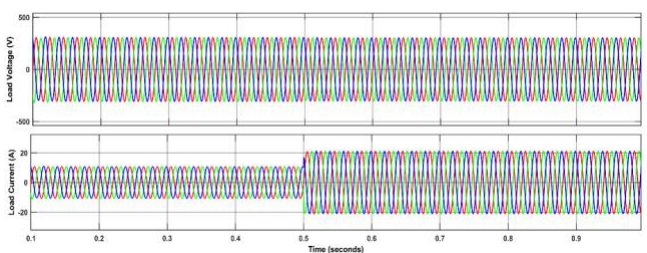
Table 3: %THD comparison

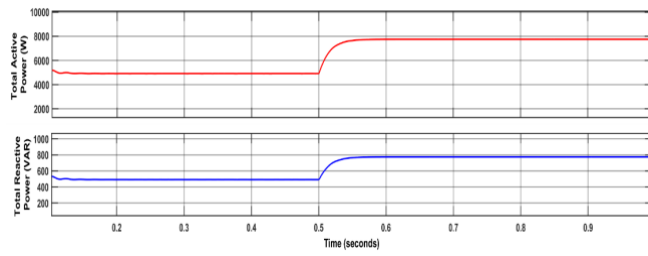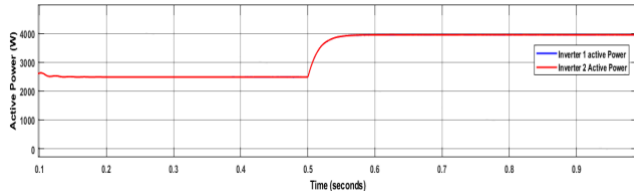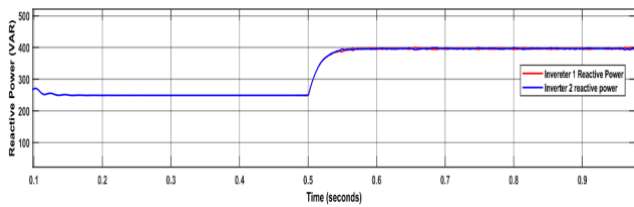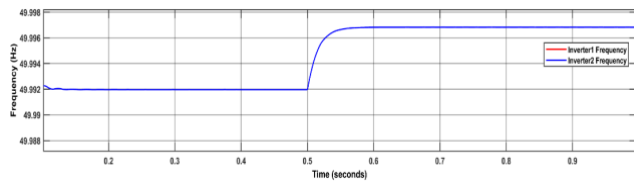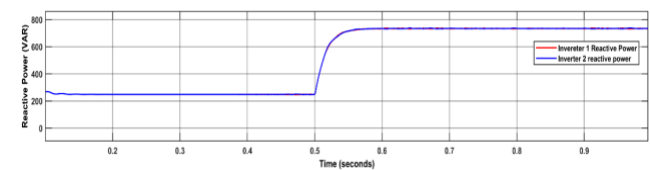| Controller	Case 1 (%)	Case 2 (%)
PI	4.21	4.79
SMC	3.52	3.07
Proposed ANNC	**1.18**	**2.30**
PIC [6]	5.480	4.21
SMC [3]	4.740	--
FLC [7]	3.650	--

(a)

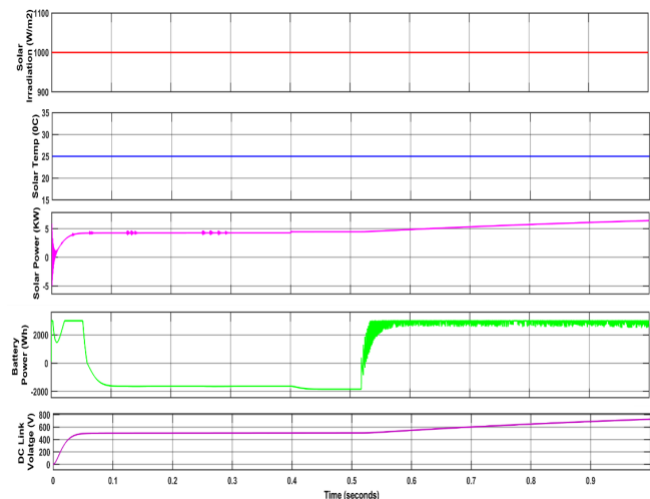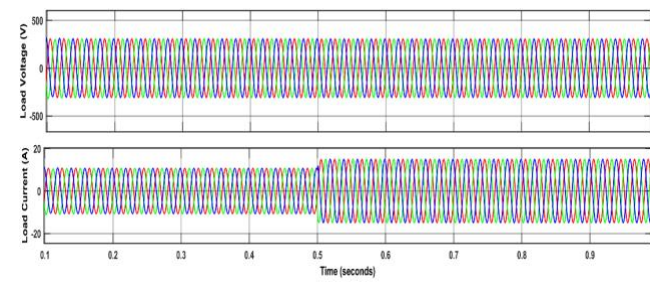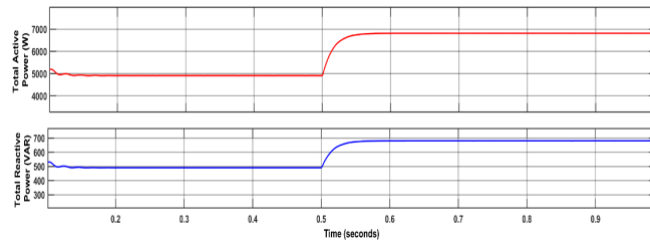
(b)

(c)
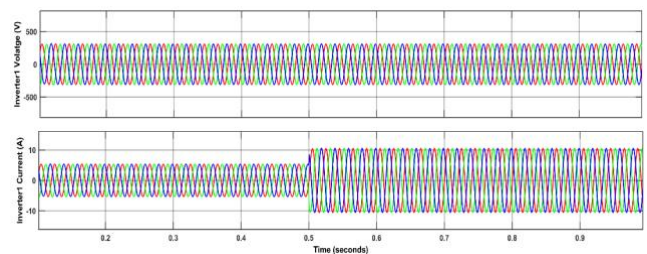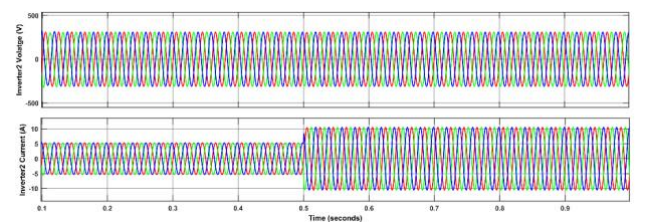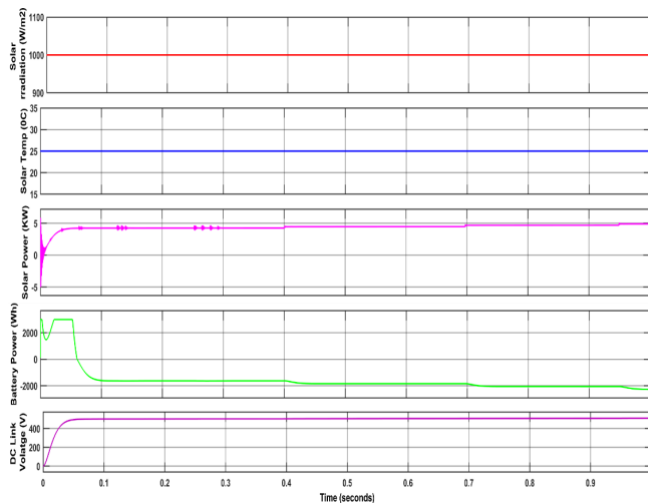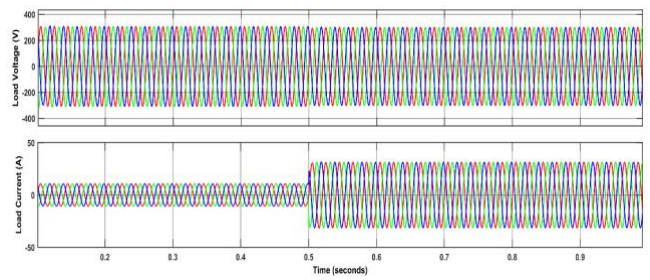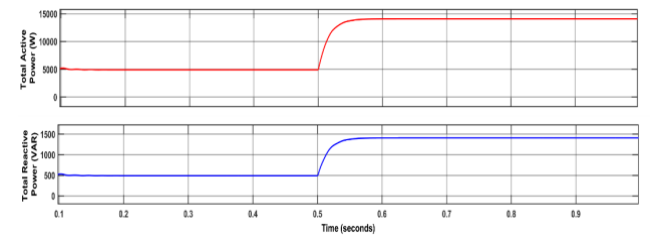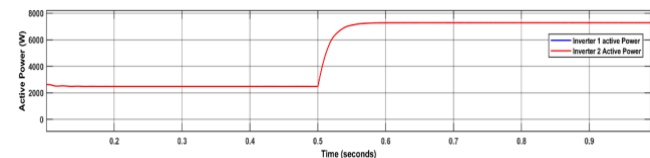
Fig. 18. (a) Inverter1 output V/I waveforms, (b) Inverter2 output V & I waveforms, (c) Load V & I waveforms, (d) Total active and reactive power waveforms (e) Active power sharing waveforms (f) Reactive power sharing waveforms (g) Frequency sharing waveform (h) Solar power, battery power with 1000w/m² irradiation and constant DCL voltage
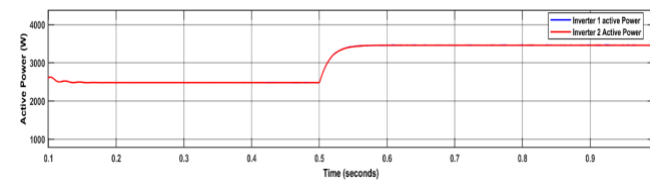
Fig. 19. (a) V & I waveforms at load, (b) Active and reactive power waveforms at load (c) Active power waveforms of inverter 1 and 2 (d) Reactive power waveforms of inverter1 and 2 (e) Solar power, battery power with 1000w/m² irradiation and 15kW load with constant DCL voltage
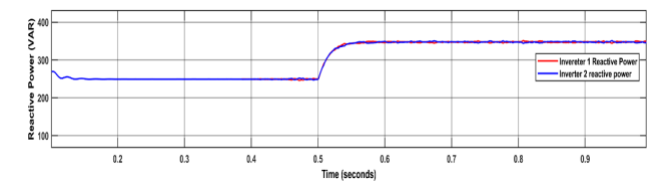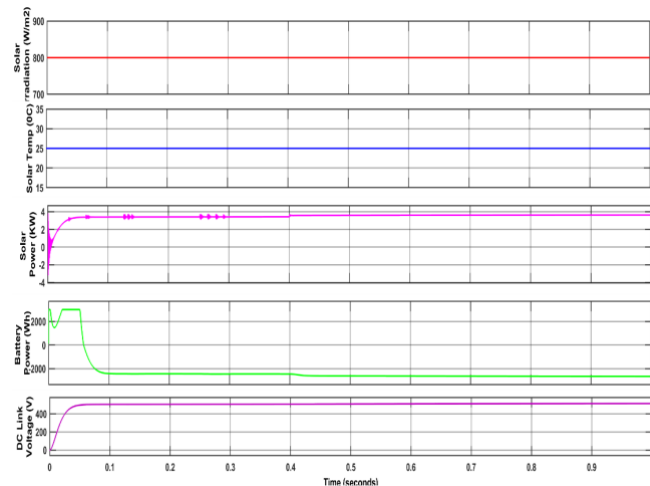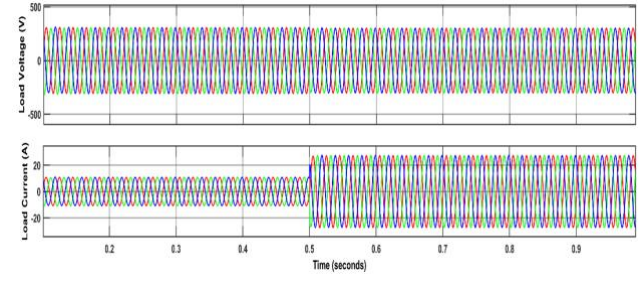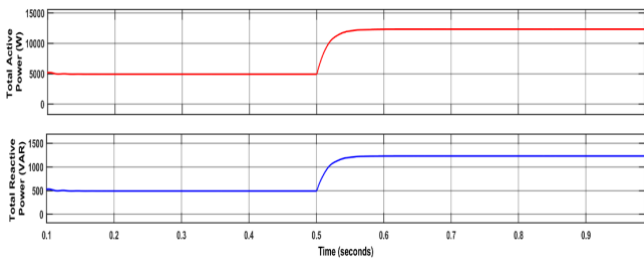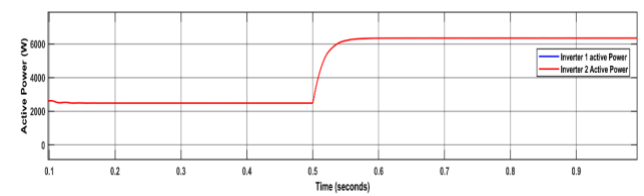
(a)

(b)

(c)

(d)

(e)

Fig. 20. (a) Voltage and current waveforms at load (b) Total active and reactive power waveforms (c) Active power sharing waveforms (d) Reactive power sharing waveforms (e) Solar power, battery power with 800w/m^2 irradiation and constant DCL voltage
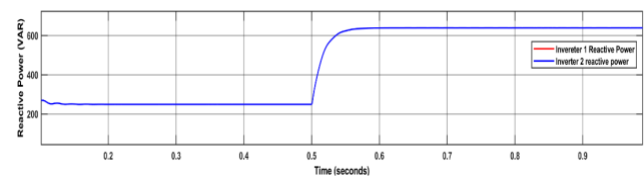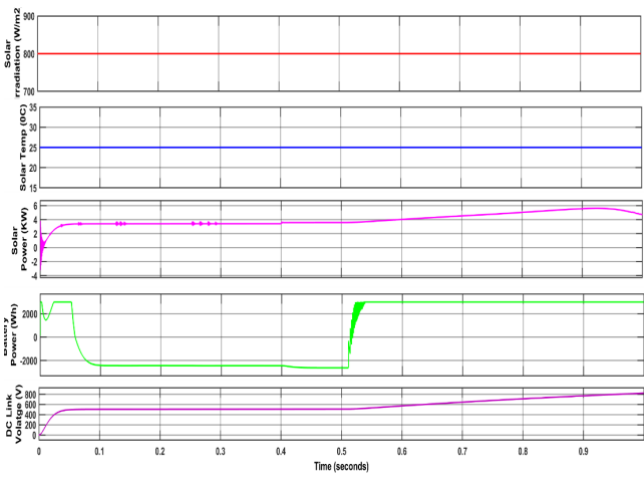

(a)

(b)

(c)

(d)

(e)

Fig. 21. (a) V & I waveforms at load, (b) Active and reactive power waveforms at load (c) Active power waveforms of inverter 1 and 2 (d) Reactive power waveforms of inverter1 and 2 (e) Solar power, battery power with 800w/m^2 irradiation and 13kW load with constant DCL voltage
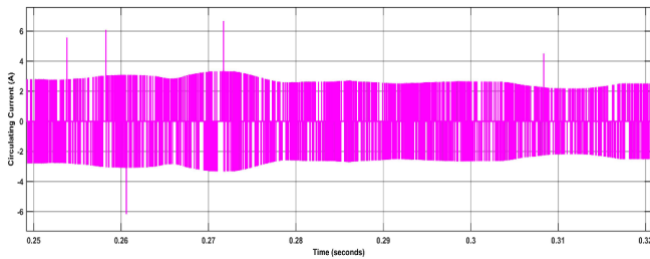
Fig.22. Circulating Current waveform
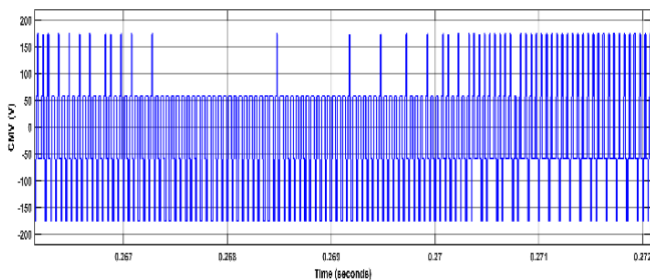

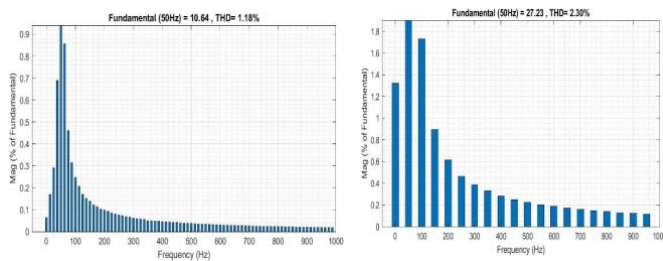**Fig.23**. Common mode voltage waveform

Fig.24. THD Spectrum

5 Conclusion

This study focused on the operation and control of a micro-grid integrated with a Parallel Connected Inverter (PCI). A new approach based on an Enhanced Droop Control (EDC) technique with ANNC controller was proposed to address the issues of suggested PCI-SBS. Performance analysis of the proposed method was conducted using the Matlab/Simulink platform with two test studies involving different loads. To highlight the viability of the developed control technique, a comparative analysis was carried out against established controllers like the PIC and SMC.

Through simulation in MATLAB, the results demonstrated excellent performance of the proposed approach in achieving multiple objectives. This includes equal power/load sharing among the two inverters, effective minimization of circulating currents (CC) and common mode voltages (CMV), as well as reduction in the total harmonic distortion (THD) of the load current. The application of the proposed technique resulted in THD values of 1.18% and 2.30% for the respective test case studies.

As a future study, it is recommended to extend this work by incorporating a hybrid controller which can further enhance the performance and efficiency of the system.

References

1. Abdelmalik Zorig, Mohammed Belkheiri, Said Barkat, Abdelhamid Rabhi & Frede Blaabjerg (2018) Sliding Mode Control and Modified SVM for Suppressing Circulating Currents in Parallel-Connected Inverters, Electric Power Components and Systems, 46:9, 1061-1071, DOI: 10.1080/15325008.2018.1466215.

2. T. Vigneysh & N. Kumarappan (2016) Artificial Neural Network Based Droop-Control Technique for Accurate Power Sharing in an Islanded Microgrid, International Journal of Computational Intelligence Systems, 9:5, 827-838, DOI: 10.1080/18756891.2016.1237183.

3. Zaidi, E., Marouani, K., Bouadi, H. et al. Circulating current reduction-based hybrid controller of an electrical drive system fed by two parallel inverters. Electr Eng 103,3049–3061 (2021). https://doi.org/10.1007/s00202-021-01284-8.

4. A. Ketabi, S. Rajamand, M. Shahidehpour, "Power Sharing in Parallel Inverters with Different Types of Loads", IET Generation, Transmission & Distribution, vol. 11, no. 10, p. 2438-2447, 2017. https://doi.org/10.1049/iet-gtd.2016.0570.

5. H. Han, X. Hou, J. Yang, J. Wu, M. Su and J. M. Guerrero, "Review of Power Sharing Control Strategies for Islanding Operation of AC Microgrids," in IEEE Transactions on Smart Grid, vol. 7, no. 1, pp. 200-215, Jan. 2016, DOI: 10.1109/TSG.2015.2434849.

6. Q. Zhang, X. Xing and K. Sun, "Space Vector Modulation Method for Simultaneous Common Mode Voltage and Circulating Current Reduction in Parallel Three-Level Inverters," in IEEE Transactions on Power Electronics, vol. 34, no. 4, pp. 3053-3066, April 2019, DOI: 10.1109/TPEL.2018.2848928.

7. I. Mehouachi, M. Abbes and S. Chebbi, "Fuzzy Logic Control of Circulating Current between Parallel Interleaved Converter Connected to Grid," 2019 16th International Multi-Conference on Systems, Signals & Devices (SSD), Istanbul, Turkey, 2019, pp. 573-577, DOI: 10.1109/SSD.2019.8893194.

8. P. Monica, M. Kowsalya, Control strategies of parallel operated inverters in renewable energy application: A review, Renewable and Sustainable Energy Reviews, Volume 65,2016, Pages 885-901, ISSN 1364-0321, https://doi.org/10.1016/j.rser.2016.06.075

9. N. Ghanbari and S. Bhattacharya, "Adaptive Droop Control Method for Suppressing Circulating Currents in DC Microgrids," in IEEE Open Access Journal of Power and Energy, vol. 7, pp. 100-110, 2020, DOI: 10.1109/OAJPE.2020.2974940.

10. Guo-Jie Li, Suleman Haider, Parallel inverter control for power sharing in islanded operation of AC micro-grid, International Journal of All Research Education and Scientific Methods (IJARESM), Volume 5, Issue 9, September- 2017.

11. Koganti Srilakshmi, Nakka Srinivas, Praveen Kumar Balachandran, Jonnala Ganesh Prasad Reddy, Sravanthy Gaddameedhi, "Design of Soccer League Optimization Based Hybrid Controller for Solar-Battery Integrated UPQC," in IEEE Access, vol. 10, pp. 107116-107136, 2022, doi: 10.1109/ACCESS.2022.3211504.

12. Koganti Srilakshmi, Sravanthy Gaddameedhi, Uday Kumar Neerati, Surender Reddy Salkuti, Ponamanenni Anoop Rao, Thattiparthi Pavan Kumar, Performance Analysis of Fuzzy-Based Controller for Wind and Battery Fed UPQC, Power Quality in Microgrids: Issues, Challenges and Mitigation Techniques. Lecture Notes in Electrical Engineering, vol 1039. Springer, Singapore. https://doi.org/10.1007/978-981-99-2066-2_11.

13. Xuan Hoa Thi Pham, Power sharing strategy in islanded microgrids using improved droop control, Electric Power Systems Research, Volume 180, 2020, 106164, ISSN 0378-7796.

14. Haider, S., Li, G. & Wang, K. A dual control strategy for power sharing improvement in islanded mode of AC microgrid. Prot Control Mod Power Syst 3, 10 (2018). https://doi.org/10.1186/s41601-018-0084-2.

15. Rahul Sharma, Sathans Suhag, Virtual impedance-based phase locked loop for control of parallel inverters connected to islanded microgrid, Computers & Electrical Engineering, Volume 73, 2019, Pages 58-70, 2018.

16. Xueguang Zhang, Tianyi Wang, Xiongfei Wang, Gaolin Wang, Zhe Chen, and Dianguo Xu, Coordinate Control Strategy for Circulating Current Suppression in Multi-Paralleled Three-Phase Inverters, IEEE Transactions on Industrial Electronics, DOI 10.1109/TIE.2016.2578280.

17. B. Wei, J. M. Guerrero, J. C. Vásquez and X. Guo, "A Circulating-Current Suppression Method for Parallel-Connected Voltage-Source Inverters with Common DC and AC Buses," in IEEE Transactions on Industry Applications, vol. 53, no. 4, pp. 3758-3769, July-Aug. 2017, doi: 10.1109/TIA.2017.2681620.

18. X. Xing, Z. Zhang, C. Zhang, J. He and A. Chen, "Space Vector Modulation for Circulating Current Suppression Using Deadbeat Control Strategy in Parallel Three-Level Neutral-Clamped Inverters," in IEEE Transactions on Industrial Electronics, vol. 64, no. 2, pp. 977-987, Feb. 2017, DOI: 10.1109/TIE.2016.2618782.

19. Shengli Huang, and Jianguo Luo, Accurate Power Sharing in Proportion for Parallel Connected Inverters by Reconstructing Inverter Output Impedance, Journal of Power Electronics, Vol. 18, No. 6, pp. 1751-1759, November2018,doi.org/10.6113/JPE.2018.18.6.1751.

20. N.S. Suresh, S. Arul Daniel, Novel droop-based controller for parallel connected solar inverter in a microgrid, Materials Today: Proceedings, Volume 46, Part 19,2021, Pages 10102-10108, ISSN 2214-7853.

21. Y. Singh, B. Singh and S. Mishra, "Control of Multiple SPV Integrated Parallel Inverters for Microgrid Applications," in IEEE Transactions on Industry Applications, vol. 59, no. 3, pp. 3700-3712, May-June 2023, DOI: 10.1109/TIA.2023.3244531.

22. Fatih Cingoz, Ali Elrayyah & Yilmaz Sozer (2015) Optimized Droop Control Parameters for Effective Load Sharing and Voltage Regulation in DC Microgrids, Electric Power Components and Systems, 43:8-10,879-889, DOI:10.1080/ 15325008. 2015. 1021 220.

23. M. Sarra, A. Belkaid, I. Colak, G. Boudechiche and K. Kayisli, " Fuzzy-MPPT Controller Based Solar Shunt Active Power Filter 2022 11th International Conference on Renewable Energy Research and Application (ICRERA), Istanbul, Turkey, 2022, pp. 436-440, doi: 10.1109/ICRERA55966.2022.9922873.

24. Ruhi Zafer Caglayan, Korhan Kayisli, Nurkhat Zhakiyev, Abdulkader Harrouz, Ilhami Colak, A Review of Hybrid Renewable Energy Systems and MPPT Methods, International journal of smart grid, Vol.6, No.3, September, 2022.

25. J. Dey, N. Mohammad and M. T. Islam, "Analysis of a Microgrid having Solar System with Maximum Power Point Tracking and Battery Energy System," 2022 10th International Conference on Smart Grid, Istanbul, Turkey, 2022, pp. 179-184.

26. M. Colak and S. Balci, Intelligent Techniques to Connect Renewable Energy Sources to the Grid: A review, 2021 9th International Conference on Smart Grid, Setubal, Portugal, 2021, pp.179-185.

27. Han Huang, Noel Bristow, Tudur Wyn David, Jeff Kettle and Grazia Todeschini, A Novel Computational Model for Organic PV Cells and Modules, International journal of smart grid Vol.4, No.4, December, 2020.